Optics and Lasers in Engineering 171 (2023) 107817

Contents lists available at ScienceDirect

Optics and Lasers in Engineering

journal homepage: www.elsevier.com/locate/optlaseng

Rhenium diselenide nanosheets as an excellent bi-color probe for intracellular two-photon imaging

Yongping Li [a], Ziyi Luo [a], Yiwan Song [a], Xiaoyu Weng [a], Yiping Wang [a], Liwei Liu [a], Jun Song [a], Junle Qu [a], Xiao Peng [a], Yufeng Yuan [a,b,*]

[a] State Key Laboratory of Radio Frequency Heterogeneous Integration, College of Physics and Optoelectronic Engineering, Shenzhen University, Shenzhen 518060, China
[b] School of Electronic Engineering and Intelligentization, Dongguan University of Technology, Dongguan 523808, China

ARTICLE INFO

Keywords:
Two-photon fluorescence probe
2D PEG@$ReSe_2$ nanosheets
High photostability
Low cytotoxicity
In vivo bicolor bioimaging

ABSTRACT

Recently two-dimensional (2D) nanomaterials-mediated photothermal therapy (PTT) has become an important tool for treating cancer. However, visually monitoring the localization of nanoagents in cancer cells remains a key challenge. Herein, exploring high photostability, and high biocompatibility probes for monitoring PTT are still highly desirable. In this study, a novel optical probe named PEG@$ReSe_2$ nanosheets (polyethylene glycol, PEG; rhenium diselenide, $ReSe_2$) was prepared and employed to perform *in vivo* two-photon imaging for monitoring PTT in esophageal cancer cells. Under the illumination of a near-infrared (NIR) femtosecond laser at 820 nm with the output power as low as 5 mW, the PEG@$ReSe_2$ nanosheets showed significant two-photon features, producing a significant photoluminescence emission band at 637 nm. In addition, the prepared PEG@$ReSe_2$ nanosheets exhibited high resistance to photobleaching. Also, the PEG@$ReSe_2$ nanosheets showed low cytotoxicity for cancer cells, providing a high viability of more than 90%. More importantly, the PEG@$ReSe_2$ nanosheets could enter cancer cells and work as a two-photon probe for visually displaying the PTT process. After 12 h incubation, the PEG@$ReSe_2$ nanosheets produced strong two-photon signals in KYSE150 cancer cells, enabling them to perform *in vivo* bi-channel bioimaging. In light of its photothermal effects, the PEG@$ReSe_2$ nanosheets also could serve as a sensor for monitoring PTT under low-power infrared laser irradiation. This study suggests that, the PEG@$ReSe_2$ nanosheets could serve as a superior two-photon biosensor for monitoring the PTT process in cancer nanomedicine.

1. Introduction

Recently advanced two-photon fluorescence (TPF) imaging has attracted worldwide attention in the biomedical field, because of its unique advantages of non-invasiveness, suppression of photodamage/phototoxicity and high penetration depth [1–3]. Under the illumination of near-infrared (NIR) light, the TPF signal with a higher frequency can be generated when fluorescent molecules simultaneously absorb two low-frequency photons [4,5]. At earlier times, water-soluble, and well-targeted two-photon organic dyes were widely applied for TPF imaging [6,7]. However, most two-photon organic dyes usually have the drawbacks of small two-photon absorption cross section and low brightness of TPF imaging, making it require high power laser for two-photon excitation [8,9]. In addition, pulsed lasers having high peak power are preferred instead of commonly used continuous lasers. In contrast to common optical imaging, two-photon-based bioimaging can effectively reduce autofluorescence, lower photobleaching and achieve high-resolution *in vivo* imaging, showing great potential in cancer diagnosis, treatment and non-invasive monitoring of drug delivery [3,10–12]. Therefore, it is of considerable significance to integrate TPF imaging approach with cancer therapy, enabling to monitor the photothermal therapy (PTT) process and evaluate therapeutic outcomes.

To date, 2D nanomaterials-mediated PTT has been considered an efficient strategy for treating cancer [13–19]. Owing to their significant absorption features in the NIR region, 2D nanoagents involved in PTT usually have good photothermal conversion ability, indicating that they can efficiently absorb a large proportion of photons and produce heat. Then, the photoluminescence performance of photothermal nanoagents would be relatively weakened. Herein, it needs to find a balance between photothermal effects and photoluminescence for photothermal

* Corresponding author at: State Key Laboratory of Radio Frequency Heterogeneous Integration, College of Physics and Optoelectronic Engineering, Shenzhen University, Shenzhen 518060, China.
E-mail address: yufengyuan@dgut.edu.cn (Y. Yuan).

https://doi.org/10.1016/j.optlaseng.2023.107817
Received 29 November 2022; Received in revised form 20 August 2023; Accepted 28 August 2023
Available online 6 September 2023

nanoagents. Meanwhile, it is of considerable importance to *real-time* monitor the dynamic localization of nanoagents for improving the outcome of PTT. Based on these observations, developing a novel optical probe with high photostability, high biocompatibility, and high bio-imaging ability in cancer cells, are highly desirable.

In the graphene family, the derivatives of graphene, such as graphene oxide and nitrogen-doped graphene, were first reported for performing TPF bioimaging, due to their large surface area and strong photoluminescence as well as high biocompatibility. For example, the derivatives of graphene not only achieve deep TPF imaging in cells and tissues, but also track specific bio-analytes via deep TPF imaging [8,20]. Afterward, a prototype member in the transition metal dichalcogenides (TMDCs) family, molybdenum disulfide (MoS_2) has been widely studied. It has been proposed that, MoS_2 nanosheets have shown photothermal effects employed for PTT [21]. In addition, functional MoS_2 quantum dots were prepared and targeted for TPF bioimaging in prostate cancer cells [22]. However, it is still difficult for monitoring the PTT process using MoS_2 quantum dots, because of its low photothermal conversion efficiency. In the phosphorene family, functional black phosphorus (BP) quantum dots were successfully employed for PTT, due to its excellent photothermal conversion efficiency [23]. However, BP quantum dots usually showed poor stability exposure to ambient air. Moreover, few-layered BP nanosheets hardly have stable photoluminescence. Thus, the member from TMDCs family has shown higher stability compared to phosphorene family.

As relatively unexplored members in TMDCs family, ReX_2 (X=S, or Se) has received considerable attention, due to its usual features. There are two forms: ReS_2, and $ReSe_2$. Similar to ReS_2, $ReSe_2$ was formed by 4 Re atoms covalently bonding with 6 Se atoms [24]. Unlike most popular members such as MoS_2 and WS_2, $ReSe_2$ exhibited significant in-plane anisotropy, and unusual electrical, and optical properties [25–27]. Moreover, the photoluminescence property of $ReSe_2$ film was studied by the single-photon excitation method. From bulk to monolayer, the photoluminescence emission of $ReSe_2$ film was slightly red-shifted from 1.29 to 1.31 eV [28]. It indicated that, the bandgap of $ReSe_2$ film was highly related tothe thickness of $ReSe_2$ film. Conversely, the ReS_2 film showed a layer-independent bandgap of 1.51 eV [29]. It is worth noting that, the narrow bandgap of $ReSe_2$ is rare in TMDs family, making it possible for exploring novel optoelectronic sensors. In addition, $ReSe_2$ showed great potential in the biomedical field. For example, Se is a biologically essential trace element, which can further enhance immune function and reduce the incidence of cancer [30,31]. To date, most fundamental studies involved in $ReSe_2$ have been mainly focused on preparation and structure modulation. To the best of our knowledge, there were no reports on $ReSe_2$ employed for *in vivo* TPF bioimaging.

Herein, we first reported a novel optical probe, namely PEG@$ReSe_2$ nanosheets, employed for *in vivo* TPF imaging in esophageal cancer cells, as shown in Fig. 1. The $ReSe_2$ nanosheets were yielded on a large scale by a top-down exfoliation approach. To enhance biocompatibility, the $ReSe_2$ nanosheets were further treated with biological polymer PEG-NH_2. Interestingly, the prepared $ReSe_2$ nanosheets showed unique TPF features under 820 nm femtosecond laser irradiation. Also, the prepared PEG@$ReSe_2$ nanosheets exhibited high resistance to photobleaching. Owing to their broad photon absorption region, the prepared PEG@$ReSe_2$ nanosheets can work as a TPF probe for performing *in vivo* bi-color bioimaging and monitoring PTT under low-power infrared laser irradiation. It indicated that, excellent two-photon signatures from PEG@$ReSe_2$ nanosheets have promising applications for *real-time* tracking PTT in biomedical field.

2. Experimental section

2.1. Chemicals and materials

In this study, all the chemicals were of the analytical grade and used without further purification. The PEG-NH_2 (MW:2000 kDa), ethanol anhydrous (97%), and n-methyl-2-pyrrolidone (NMP, 99%, Reagent Plus) were bought from Shanghai Ponsure Biotech, Inc, Aladdin Company, and Sigma-Aldrich, respectively. The cells culture media containing RPMI Medium Modified (RPMI1640, 99%), Dulbecco minimum essential medium (DMEM, 99%), phosphate buffered saline (PBS), and fetal bovine serum (FBS, 99%) were purchased from Hyclone. Live & Dead Cell Double Staining Kit and cell Counting Kit-8 (CCK-8, 99.9%) assay kits were purchased from KeyGen BioTech. The $ReSe_2$ crystal (99.9%) was bought from HQ Graphene Company (Netherlands). Ultrapure water with a resistivity of 18.2 MΩ/cm was employed to wash and dissolve PEG@$ReSe_2$ nanosheets.

2.2. Fabrication of PEG@$ReSe_2$ nanosheets

The $ReSe_2$ nanosheets were fabricated by an ultrasonication-assisted liquid phase exfoliation method [32]. Both 12 mg bulk $ReSe_2$ and 80 mL NMP solvent were added into a beaker. Then, the bulk $ReSe_2$ in NMP was treated with continuous probe sonication (JY98-IIIDV, SCIENTZ) for 38 h with the help of an ice bath. To avoid local high temperature generated by probe sonication, there was a sonication delay. For each ultrasonication period, the turn-on time of probe was 2 s, and the turn-off time was 6 s. Afterward, the obtained mixture was first centrifuged at

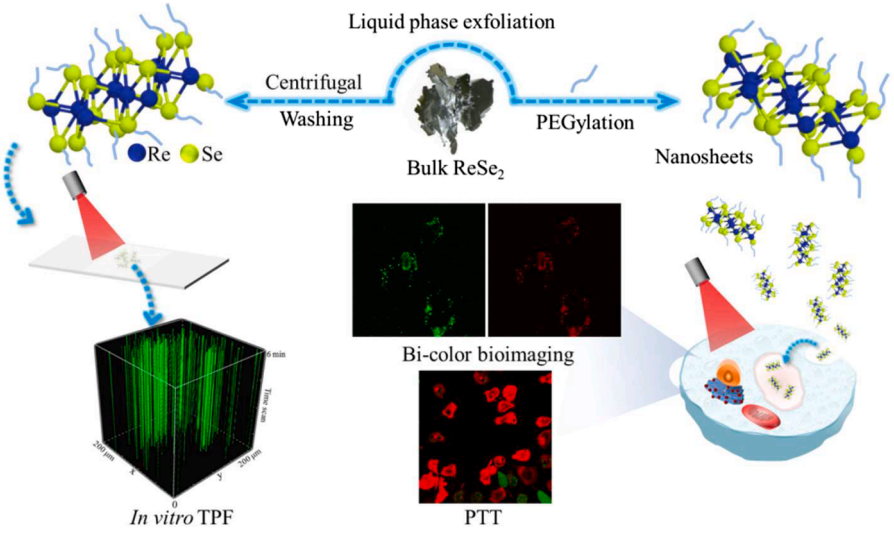

Fig. 1. Schematic illustration of PEG-$ReSe_2$ nanosheets employed for *in vivo* bi-color TPF bioimaging in PTT.

6000 rpm for 18 min to remove large-sized $ReSe_2$ nanosheets. To obtain small-sized $ReSe_2$ nanosheets, the obtained supernatant was further washed by centrifugation at 14300 rpm for 18 min. Finally, the small-sized $ReSe_2$ nanosheets were yielded by washing twice with ethanol and ultra-pure water, respectively.

In order to optimize the stability and solubility in different physiological conditions, as well as biocompatibility and low cytotoxicity of prepared $ReSe_2$ nanosheets, the polymer PEG-NH_2 was utilized to modify the surface of small-sized $ReSe_2$ nanosheets. It is worth noting that, poly ethylene glycol (PEG) are a class of biocompatible polymers, which can make nanoagents facilitate tumor targeting. In addition, the surface charge of ReS_2 nanosheets functionalized by PEG-NH_2 moiety is positive. For the negatively charged surface of cell membrance, the strong electrostatic interaction force can significantly develop the cellular uptake behavior. Moreover, PEG-NH_2-decorated nanoagents have shown high bio compatibility [23,32]. In brief, the PEG-NH_2 molecules (50 mg) were added into ultra-pure water containing small-sized $ReSe_2$ nanosheets, and stirred continuously for 12 h. Then, the mixture was centrifuged and washed 3 times at 14300 rpm to remove the excess PEG-NH_2 molecules. Finally, the water-soluble PEG@$ReSe_2$ nanosheets were yielded into 1 mL ultra-pure water for further experiments.

2.3. Material characterization

An ultraviolet-visible spectrophotometer (UV-1780, SHIMADZU) was employed to measure the absorbance of PEG@$ReSe_2$ nanosheets in different concentrations. Both the thickness and topography of prepared PEG@$ReSe_2$ nanosheets were characterized by atomic force microscopy (AFM, Dimension ICON, Brooke) and transmission electron microscopy (TEM, HITACH HT7700), respectively. The element composition of PEG@$ReSe_2$ nanosheets was measured by X-ray photoelectron spectroscopy (XPS, Thermo Scientific NEXSA, USA). The Raman spectra of PEG@$ReSe_2$ nanosheets were obtained by a confocal Raman spectrometer (inVia, Renishaw, UK).

2.4. TPF features of PEG@$ReSe_2$ nanosheets

To study the TPF features of PEG@$ReSe_2$ nanosheets, a broad femtosecond laser (Chameleon Discovery, 80 MHz, Coherent Company) with tunable NIR excitation wavelengths (820–1300 nm) was employed. To determine the photoluminescence emission of PEG@$ReSe_2$ nanosheets, a spectrometer (Ocean Optics, USB2000) was applied to record photoluminescence spectra excited by tunable excitation wavelengths ranging from 820 to 900 nm. Additionally, the photoluminescence lifetime of PEG@$ReSe_2$ nanosheets was determined under an excitation wavelength of 820 nm.

To study the feasibility of bioimaging ability of PEG@$ReSe_2$ nanosheets, a Nikon confocal scanning inverted microscopy that consists of A1R MP+ and Carl Zeiss, LSM 800 with Airyscan modules, was employed using a 60× oil immersion objective. It is worth noting that, there were two imaging channels employed for collecting photons with different frequencies. For example, Channel 1 responds to the spectra interval from 512 to 558 nm, and Channel 2 stands for the spectra interval from 577 to 633 nm. To measure *in vitro* TPF signals of PEG@$ReSe_2$ nanosheets, 20 μL lowconcentration PEG@$ReSe_2$ nanosheet solution was dropped on a glass slide, and the PEG@$ReSe_2$ nanosheets were allowed to dry naturally at room temperature.

To investigate *in vivo* TPF imaging effect of PEG@$ReSe_2$ nanosheets, 400 μL 100 μg/mL PEG@$ReSe_2$ nanosheets were incubated with KYSE150 cancer cells in 8-well plates in an incubator for 12 h. After washing with PBS, the TPF intensity of PEG@$ReSe_2$ nanosheets in KYSE150 cells was continuously monitored by a Nikon confocal microscope.

The photothermal killing effects of PEG@$ReSe_2$ nanosheets were characterized by Live & Dead Cell Double Staining Kit. In brief, 200 μL work solutions (8 μM PI, 2 μM Calcein-AM) were mixed into KYSE150 cancer cells incubated with PEG@$ReSe_2$ nanosheets. After 30 min, KYSE150 cancer cells incubated with PEG@$ReSe_2$ nanosheets were continuously irradiated with a femtosecond laser for 10 min at 820 nm. After laser illumination, the cancer cells stained with green fluorescence were alive, and the cancer cells labeled with red fluorescence were killed by photothermal effects.

2.5. In vivo cellular toxicity of PEG@$ReSe_2$ nanosheets

The cellular toxicity of PEG@$ReSe_2$ nanosheets was studied utilizing the standard CCK-8 assay. The procedure was performed as follows: cells in 96-well plates ($\approx 1 \times 10^4$ cells per well) were cultured in fresh medium containing different concentrations of PEG@$ReSe_2$ (0, 50, 100, 200, and 400 μg/mL). After 12 h incubation, both KYSE150 and HeLa cells were cleaned several times using PBS for removing residual PEG@$ReSe_2$ nanosheets. Then, a fresh culture medium containing CCK-8 (1:10 ratio of CCK-8 to culture medium) was injected into 96-well plates. After 1 h incubation, the light density values of KYSE150 and HeLa cells at 450 nm were recorded with a microplate reader.

3. Results and discussion

As the bulk $ReSe_2$ is stacked by weak van der Waals forces in the interlayer, few-layered $ReSe_2$ nanosheets can be obtained by a peeling method. With the assistance of probe ultrasound and ice-water bath, the $ReSe_2$ nanosheets were continuously exfoliated from $ReSe_2$ crystal in NMP, as shown in Fig. 2A. The large-sized nanosheets can be removed by centrifugal cleaning at 8000 rpm, guaranteeing that the obtained $ReSe_2$ nanosheets are highly dispersed and homogeneous in size. To further enhance the dispersibility and biocompatibility of $ReSe_2$ nanosheets in physiological solutions, the polymer PEG-NH_2 molecules were applied to decorate with small-sized $ReSe_2$ nanosheets obtained by centrifugal cleaning at 14300 rpm. As shown in Fig. 2B, the freshly prepared PEG@$ReSe_2$ nanosheets showed good dispersibility in three solutions such as ultra-pure water, PBS, and cells medium. In addition, the quantitative absorbance (Fig. 2B) from PEG@$ReSe_2$ nanosheets in various concentrations also showed good dispersibility.

In particular, our prepared PEG@$ReSe_2$ nanosheets exhibited a strong absorption in the NIR region (Fig. 2B). Fig. 2C–E showed the elemental composition and bonding configurations of prepared PEG@$ReSe_2$ nanosheets measured by XPS, where the binding energy of Re and Se elements are consistent with previous reports [33–35]. In addition, Raman spectroscopy was carried out to perform fingerprint identification of PEG@$ReSe_2$ nanosheets, as shown in Fig. 2F. It can be found that, the characteristic Raman band at 124 cm^{-1} belongs to the in-plane E_g-like mode, and the two Raman band located at 159, and 172 cm^{-1} is ascribed to the out-of-plane A_g-like mode [28,36,37]. Finally, both TEM (Fig. 2G) and AFM images (Fig. 2H) clearly showed that, the average size of PEG@$ReSe_2$ nanosheets was determined to be 43 nm (Fig. 2I), satisfying the size requirements (less than 200 nm) for endocytosis. However, the yield of small size $ReSe_2$ nanosheets is highly dependent on the ultrasound time, ultrasound power and probe diameter [38]. In this study, the yield of small-sized $ReSe_2$ nanosheets (~43 nm) was about 20% by controlling the sonication time (38 h), sonication power (400 W), probe diameter (20 mm), and centrifugation speed (6000 rpm, 18 min; 14300 rpm, 18 min).

Next, the photoluminescence features of PEG@$ReSe_2$ nanosheets were studied using a NIR tunable wavelength femtosecond laser, as illustrated in Fig. 3. When the femtosecond laser excitation wavelength was tunable between 820 and 900 nm, there was a stable photoluminescence band located at 637 nm. It indicates that, the photoluminescence band of PEG@$ReSe_2$ nanosheets was independent of the excitation wavelength. To verify the detectable band at 637 nm belonged to TPF, the relationship based on photoluminescence intensity *vs.* excitation powder at 820 nm was plotted, as shown in Fig. 3B. There

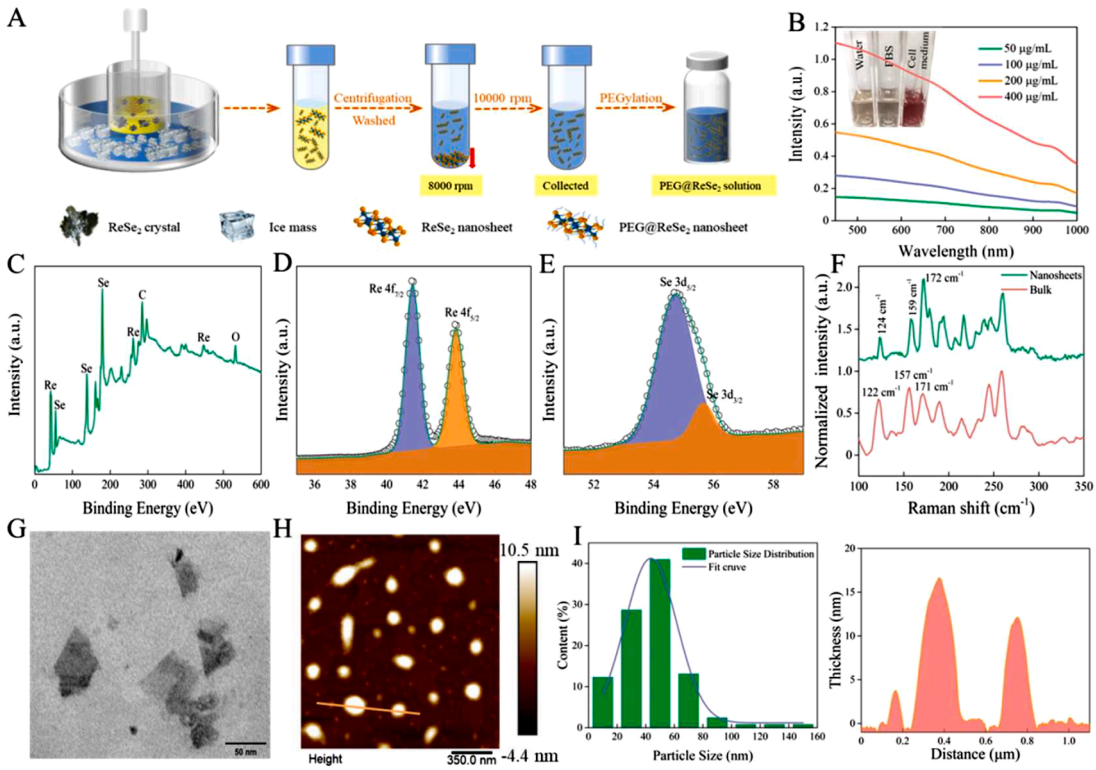

Fig. 2. Preparation and characterization of PEG@$ReSe_2$ nanosheets. A Preparation procedure of PEG@$ReSe_2$ nanosheets. B Absorption spectra of PEG@$ReSe_2$ nanosheets in different concentrations (0, 50, 100, 200, and 400 μg/mL. Inset: photographs of PEG@$ReSe_2$ nanosheets in three solvents such as ultra-pure water, PBS and cell medium, respectively). C–E XPS spectrum of PEG@$ReSe_2$ nanosheets. F Raman spectra of PEG@$ReSe_2$ nanosheets and $ReSe_2$ bulk. G TEM images of PEG@$ReSe_2$ nanosheets. H AFM image PEG@$ReSe_2$ nanosheets. I Particle size and thickness distribution of PEG@$ReSe_2$ nanosheets.

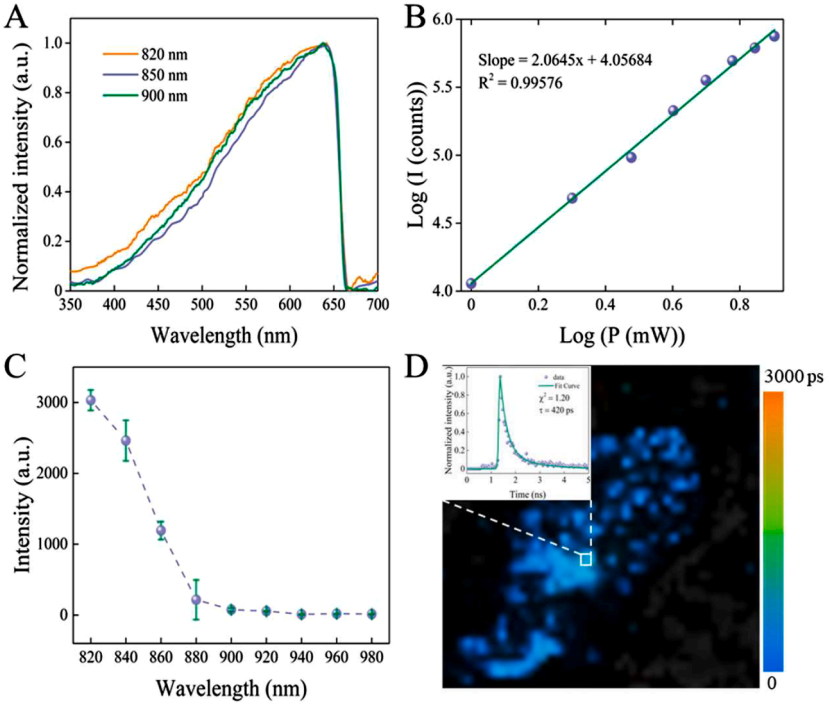

Fig. 3. A TPF spectra of PEG@$ReSe_2$ nanosheets obtained by various excitation wavelengths at 820, 850, and 900 nm. B Logarithmic relationship between TPF intensity at 637 nm and excitation power. C Related TPF intensity of PEG@$ReSe_2$ nanosheets obtained by different excitation wavelengths under the same power. D Photoluminescence lifetime image of PEG@$ReSe_2$ nanosheets under the excitation of 820 nm. The inset was fitting curve of lifetime.

was a fitted slope of 2.0654, showing that, the photoluminescence band at 637 nm was from two-photon excitation. In addition, the TPF intensity of PEG@$ReSe_2$ nanosheets was measured by changing the different excitation wavelengths from 820 to 980 nm under the same output power (6 mW), as shown in Fig. 3C. As the excitation wavelength is fixed at 820 nm, it can generate the strongest photoluminescence band. Moreover, Fig. 3D indicated that, the TPF lifetime of PEG@$ReSe_2$ nanosheets was determined to be 420 picoseconds (ps) via a double exponential decay fitting.

Recently, multicolor fluorescence imaging with single photon excitation has been widely studied, due to its advantages of providing multichannel bioimaging information. To date, a host of emitting materials, such as organic fluorescent dyes and semiconductor quantum dots have been proposed [39–42]. However, they usually suffer from the drawback of single-photon excitation, resulting in potential photobleaching and low imaging depth. Conversely, the broad photoluminescence band of PEG@$ReSe_2$ nanosheets suggests that, it has the potential for multichannel photoluminescence imaging, furthering improve spatial localization and resolution of bioimaging.

Considering that the TPF of PEG@$ReSe_2$ nanosheets is not sensitive to variation of excitation wavelength, the excitation wavelength in NIR-I can be selected. Fig. 3C showed that, with the same excitation power, the TPF intensity of PEG@$ReSe_2$ nanosheets rapidly decreases as the excitation wavelength approaches to be 900 nm. However, the strong TPF signal was still present at 900 nm. Compared to multicolor fluorescence imaging produced by multi-dyes loaded nanomaterials, PEG@$ReSe_2$ nanosheets show greater potential for bioimaging applications.

An excellent TPF sensor should be having good photostability exposure to the irradiation of a femtosecond laser. Thus, the photostability of PEG@$ReSe_2$ nanosheets was studied, as shown in Fig. 4A–D. After 100 scans, no significant variation was observed in the intensity of TPF for PEG@$ReSe_2$ nanosheets. It indicates that it can bear photobleaching. Moreover, three-dimensional TPF imaging of PEG@$ReSe_2$ nanosheets (Fig. 4E) showed that, it is suitable for *in vivo* TPF imaging in cancer cells.

Prior to *in vivo* imaging in live cancer cells, we studied the cytotoxicity of PEG@$ReSe_2$ nanosheets by employing a CCK-8 kit. After 24 h incubation with different concentrations of PEG@$ReSe_2$ nanosheets solutions, the cell viability of HeLa cells and KYSE150 cells were still more than 90%, even as the PEG@$ReSe_2$ nanosheets concentrations were as high as 400 μg/mL (Fig. 4F). These observations suggests that, our prepared PEG@$ReSe_2$ nanosheets have high biocompatibility and low cytotoxicity, because of the surface modification of polymer PEG-NH_2.

Afterward, *in vivo* bioimaging capability of PEG@$ReSe_2$ nanosheets was performed in KYSE150 cancer cells. In the absence of PEG@$ReSe_2$ nanosheets, there was no detectable two-photon signal in KYSE150 cancer cells under the illumination of 5 mW femtosecond laser at 820 nm, as shown in Fig. 5 (Case 1). As the power of the femtosecond laser at 820 nm was as high as 40 mW, the weak TPF signal from KYSE150 cancer cells was obtained in Channel 1 (512–558 nm, Case 2, Fig. 5). However, the strong TPF images (Case 3, Fig. 5) of PEG@$ReSe_2$ nanosheets in KYSE150 cancer cells were produced by a femtosecond laser at 820 nm as low as 5 mW. Moreover, the TPF signals appeared in both Channel 1 and Channel 2, clearly showed the outline of KYSE150 cancer cells. It means that, the PEG@$ReSe_2$ nanosheets can enter KYSE150 cancer cells through endocytosis. Compared with the intensity of TPF signals in KYSE150 cancer cells, the intensity of TPF signals from PEG@$ReSe_2$ nanosheets PEG@$ReSe_2$ nanosheets was enhanced by almost 18 times. To determine the imaging depth, the penetration depth of TPF signals in KYSE150 cells was measured to be 12.3 μm (Case 4, Fig. 5) via the Z-scan technique. It can be found that, the PEG@$ReSe_2$ nanosheet can stain the entire KYSE150 cancer cells and exhibit a clear TPF image. Moreover, Moreover, the 3D TPL images (Case 4, Fig. 5) of PEG@$ReSe_2$ nanosheets incubated with cancer cells clearly showed that, the PEG@$ReSe_2$ nanosheets in cancer cells has a significant distribution depending on imaging depth. When the focal plane was scanned into the middle layer of cancer cells, the TPL signals from PEG@$ReSe_2$ nanosheets can be still detected. Based on this observation, it can be deduced that, the PEG@$ReSe_2$ nanosheets have entered cancer cell interior through endocytosis. Therefore, the PEG@$ReSe_2$ nanosheets have good permeability. Thanks to the broad TPF spectrum of PEG@$ReSe_2$ nanosheets, bi-color TPF imaging can be achieved in KYSE150 cells, indicating that PEG@$ReSe_2$ nanosheets have great promising in *in vivo* bicolor TPF imaging in living cells. Compared with MoS_2 quantum dots (QDs) with a photofluorescence emission at 430 nm [43], the two-photon emission spectrum of $ReSe_2$ nanosheets is located at 637 nm, showning has lower scattering and absorption of photons. More importantly, $ReSe_2$ nanosheets can be employed to perform dual-channel bioimaging in a low-power excitation condition,

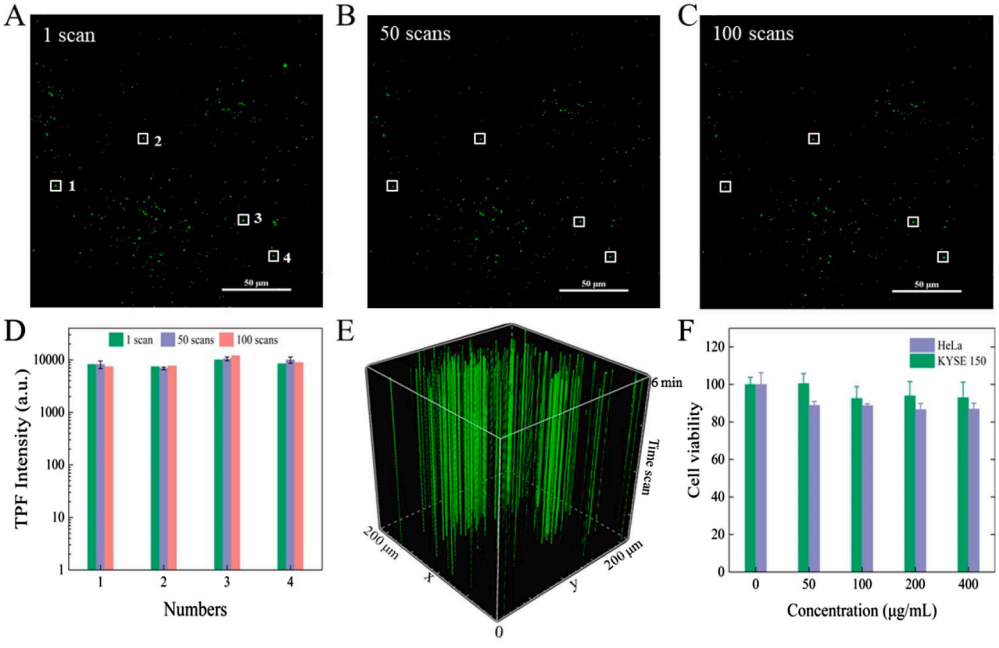

Fig. 4. *In vitro* TPF images of PEG@$ReSe_2$ nanosheets obtained from various scans under the illumination of femtosecond laser at 820 nm with an output power of 3 mW. Noting that, each scan takes ~2.1 s. A 1 scan; B 50 scans; C 100 scans; D Variations in TPF intensity of PEG@$ReSe_2$ nanosheets (selected 4 points) experiencing different numbers of scans corresponds to Fig. 4A–C. E Three-dimensional TPF image of PEG@$ReSe_2$ nanosheets; F *In vivo* cells viability of KYSE150 and HeLa treated with different concentrations (0, 50, 100, 200, and 400 μg/mL) of PEG@$ReSe_2$ nanosheets. The scale bar is 50 μm.

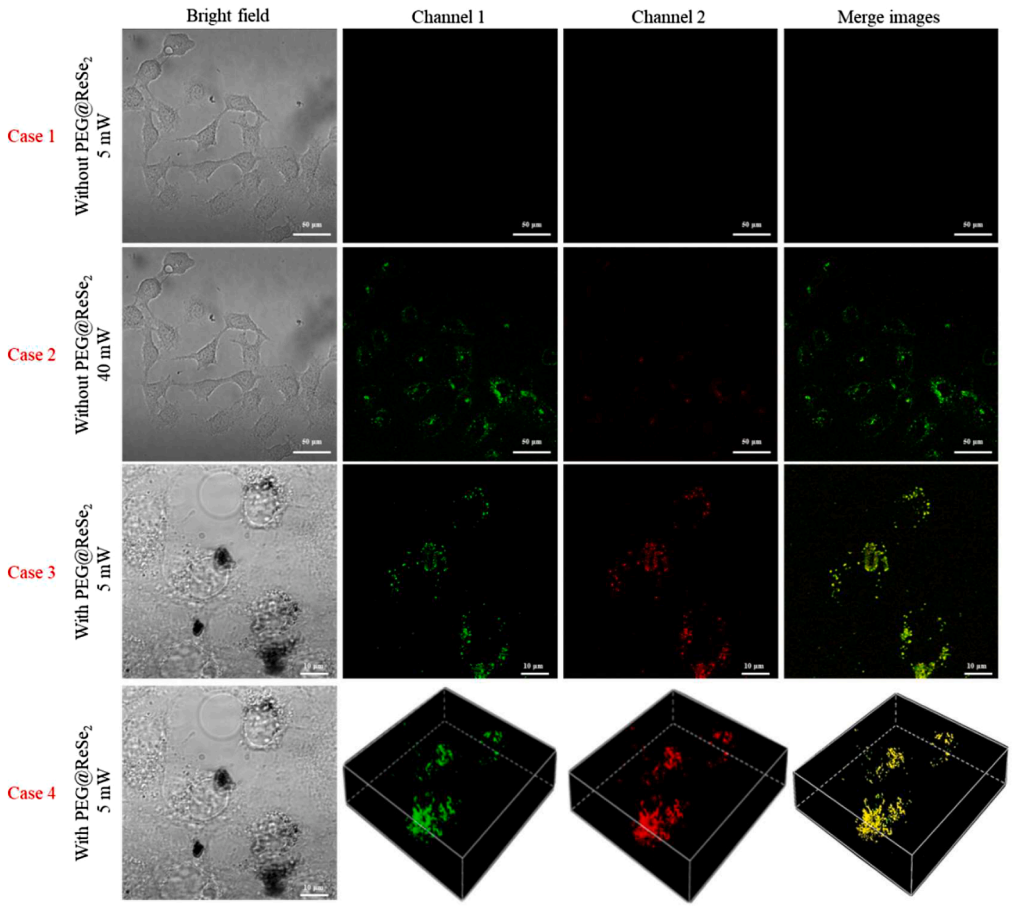

Fig. 5. TPF images of KYSE150 cells spontaneously photoluminescent (first and second rows) and incubated with PEG@$ReSe_2$ nanosheets (100 μg/mL, third and fourth rows) under different power fs pulsed laser irradiation at 820 nm. TPF microscopy image from channel 1 at 512–558 nm and channel 2 at 577–633 nm.

producing higher imaging resolution and brightness.

Finally, the feasibility of PEG@$ReSe_2$ nanosheets employed for monitoring PTT was studied, as shown in Fig. 6. In the absence of PEG@$ReSe_2$ nanosheets, the KYSE150 cancer cells were continuously irradiated for 10 min by a femtosecond laser at 820 nm. When the power was 10 mW, the viability of KYSE150 cancer cells was almost 100% (Case 1). As the power was increased to be 45 mW, almost 40% of KYSE150 cancer cells were killed (Case 2). Owing to excellent absorption capability for NIR photons, the PEG@$ReSe_2$ nanosheets can produce a significant photothermal effect on KYSE150 cancer cells. When the power was 5 mW, the KYSE150 cancer cells can be efficiently killed (Case 3). Unlike MoS_2 QDs, $ReSe_2$ nanosheets have significant photon absorption in a NIR region (Fig. 2(B)), indicating that the photothermal conversion efficiency of $ReSe_2$ nanosheets should be higher than that of previously reported MoS_2 QDs.

Under the irradiation of an ultrafast pulsed laser, the PEG@$ReSe_2$ nanosheets can generate a host of hot carriers and electrons by the two-photon absorption. Therefore, the temperature of the PEG@$ReSe_2$ nanosheets increases instantaneously, accompanied by hot carriers recombining and releasing energy in PEG@$ReSe_2$ nanosheet lattice [44]. One can conclude that, PEG@$ReSe_2$ nanosheets can be employed for intracellular TPF imaging in living cells, and it also works as an excellent photothermal nanoagents for PTT. In light of these observations, with the help of the TPF bioimaging method, the dynamic localization of PEG@$ReSe_2$ nanosheets in cancer cells can be visually monitored to further evaluate the therapeutic outcomes of PTT.

4. Conclusions

In this study, we successfully prepared a novel TPF probe named PEG@$ReSe_2$ nanosheets, which can be employed to visually monitor the localization dynamics of PEG@$ReSe_2$ nanosheets in cancer cells by *in vivo* TPF bioimaging. Under the NIR illumination of pulsed laser, PEG@$ReSe_2$ nanosheets exhibited a broad TPF emission from ultraviolet to visible region. And the detectable TPF band was located at 637 nm, showing independent on excitation light. In addition, the PEG@$ReSe_2$ nanosheets have shown high photostability, enable to efficiently prevent from photobleaching. Moreover, low *in vivo* toxicity of PEG@$ReSe_2$ nanosheets makes it work as a good probe in living cells. More importantly, when PEG@$ReSe_2$ nanosheets were incubated with KYSE150 cancer cells, *in vivo* bi-color TPF bioimaging can be achieved under a low power of 5 mW. In the process of TPF bioimaging, PEG@$ReSe_2$ nanosheets can also produce photothermal effects to kill KYSE150 cancer cells. With the help of the TPF bioimaging method, it is possible to visually monitor the location of PEG@$ReSe_2$ nanosheets in the PTT process. It can be expected that, PEG@$ReSe_2$ nanosheets have great potential for performing TPF bioimaging in living cells. Meanwhile, PEG@$ReSe_2$ nanosheets also have promising applications for monitoring PTT process and evaluating therapeutic outcomes in early cancer microsurgery.

CRediT authorship contribution statement

Yongping Li: Investigation, Visualization, Resources, Writing – original draft. **Ziyi Luo:** Investigation. **Yiwan Song:** Visualization. **Xiaoyu Weng:** Formal analysis. **Yiping Wang:** Formal analysis. **Liwei**

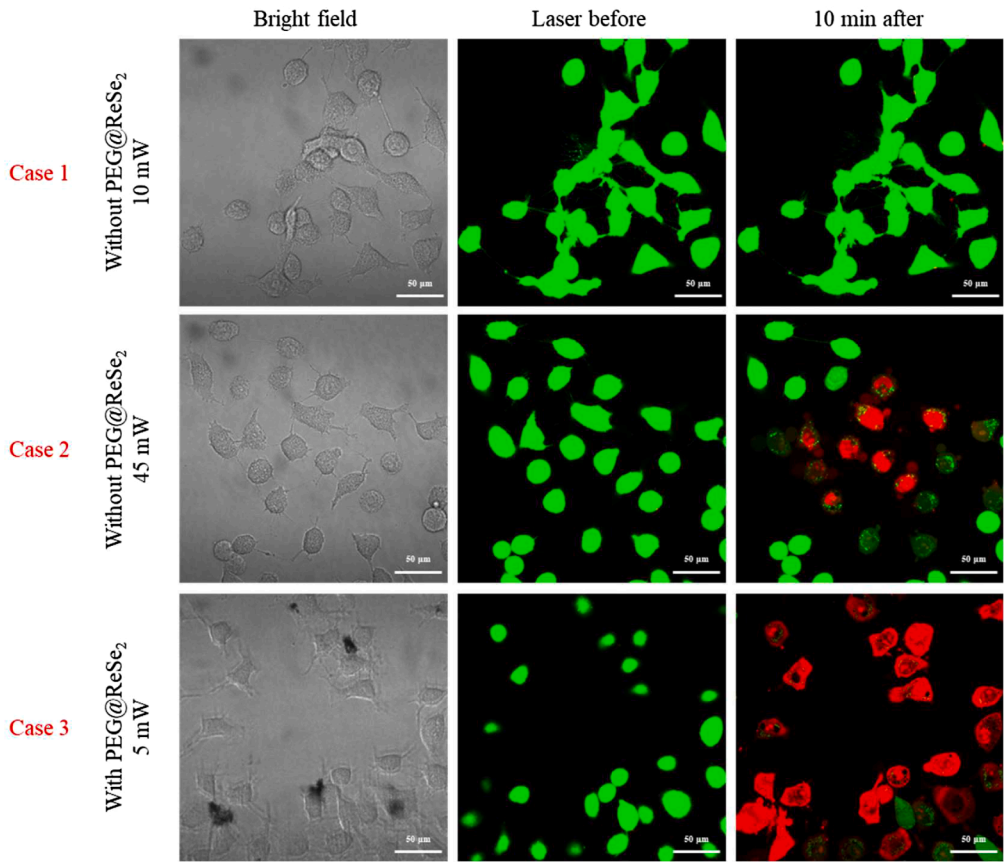

Fig. 6. Viability of KYSE150 cells treated with PEG@$ReSe_2$ nanosheets (100 μg/mL) under the illumination of fs pulse laser at 820 nm with a power of 5 mW. The Control is KYSE150 cells treated without the addition of PEG@$ReSe_2$ nanosheets. The scale bar is 50.0 μm.

Liu: Formal analysis. **Jun Song:** Formal analysis. **Junle Qu:** Formal analysis. **Xiao Peng:** Formal analysis, Supervision. **Yufeng Yuan:** Formal analysis, Writing – review & editing, Supervision.

Declaration of Competing Interest

The manuscript has been read and approved by all authors, and all authors have agreed to be considered for publication in *Optics and Lasers in Engineering*. All authors declare that they do not have any competing interests in the final manuscript with the title of " Rhenium Diselenide Nanosheets as an Excellent Bi-color Probe for Intracellular Two-Photon Imaging ".

Data availability

Data will be made available on request.

Acknowledgments

This work was partially supported by the National Key R&D Program of China (2021YFF0502900), the National Natural Science Foundation of China (62075137/31771584/61835009/62175161), the Guangdong Basic and Applied Basic Research Foundation (2020A1515010377/2022A1515011845), Shenzhen Basic Research Program (JCYJ20210324095810028), Dongguan Science and Technology of Social Development Program (20231800936312), the high-level talent program of Dongguan University of Technology (No. 221110080).

References

[1] Liu Q, Guo B, Rao Z, Zhang B, Gong JR. Strong two-photon-induced fluorescence from photostable, biocompatible nitrogen-doped graphene quantum dots for cellular and deep-tissue imaging. Nano Lett 2013;13:2436–41.
[2] Bobba KN, Won M, Shim I, Velusamy N, Yang Z, Qu J, Kim JS, Bhuniya S. A BODIPY-based two-photon fluorescent probe validates tyrosinase activity in live cells. Chem Commun 2017;53:11213–6.
[3] Yi R, Das P, Lin F, Shen B, Yang Z, Zhao Y, Hong L, He Y, Hu R, Song J. Fluorescence enhancement of small squaraine dye and its two-photon excited fluorescence in long-term near-infrared I&II bioimaging. Opt Express 2019;27:12360–72.
[4] Huang C, Qu J, Qi J, Yan M, Xu G. Dicyanostilbene-derived two-photon fluorescence probe for free zinc ions in live cells and tissues with a large two-photon action cross section. Org Lett 2011;13:1462–5.
[5] Yan W, Huang Y, Wang L, Guo Y, Li J, Zhu Y, Yang Z, Qu J. Aberration correction to optimize the performance of two-photon fluorescence microscopy using the genetic algorithm. Microsc Microanal 2022;28:383–9.
[6] Xu C, Zipfel W, Shear JB, Williams RM, Webb WW. Multiphoton fluorescence excitation: new spectral windows for biological nonlinear microscopy. Proc Natl Acad Sci 1996;93:10763–8.
[7] Stosiek C, Garaschuk O, Holthoff K, Konnerth A. *In vivo* two-photon calcium imaging of neuronal networks. Proc Natl Acad Sci 2003;100:7319–24.
[8] Zheng Z, Zhang T, Liu H, Chen Y, Kwok RT, Ma C, Zhang P, Sung HH, Williams ID, Lam JW. Bright near-infrared aggregation-induced emission luminogens with strong two-photon absorption, excellent organelle specificity, and efficient photodynamic therapy potential. ACS Nano 2018;12:8145–59.
[9] Wu L, Liu J, Li P, Tang B, James TD. Two-photon small-molecule fluorescence-based agents for sensing, imaging, and therapy within biological systems. Chem Soc Rev 2021;50:702–34.
[10] Gu B, Wu W, Xu G, Feng G, Yin F, Chong PHJ, Qu J, Yong KT, Liu B. Precise two-photon photodynamic therapy using an efficient photosensitizer with aggregation-induced emission characteristics. Adv Mater 2017;29:1701076.
[11] Pliss A, Peng X, Liu L, Kuzmin A, Wang Y, Qu J, Li Y, Prasad PN. Single cell assay for molecular diagnostics and medicine: monitoring intracellular concentrations of macromolecules by two-photon fluorescence lifetime imaging. Theranostics 2015;5:919.
[12] Samanta S, Huang M, Li S, Yang Z, He Y, Gu Z, Zhang J, Zhang D, Liu L, Qu J. AIE-active two-photon fluorescent nanoprobe with NIR-II light excitability for highly efficient deep brain vasculature imaging. Theranostics 2021;11:2137.

[13] Miao ZH, Lv LX, Li K, Liu PY, Li Z, Yang H, Zhao Q, Chang M, Zhen L, Xu CY. Liquid exfoliation of colloidal rhenium disulfide nanosheets as a multifunctional theranostic agent for *in vivo* photoacoustic/CT imaging and photothermal therapy. Small 2018;14:1703789–17037800.
[14] Li M, Yang X, Ren J, Qu K, Qu X. Using graphene oxide high near-infrared absorbance for photothermal treatment of Alzheimer's disease. Adv Mater 2012; 24:1722–8.
[15] Naguib M, Kurtoglu M, Presser V, Lu J, Niu J, Heon M, Hultman L, Gogotsi Y, Barsoum MW. Two-dimensional nanocrystals produced by exfoliation of Ti_3AlC_2. Adv Mater 2011;23:4248–53.
[16] Cheng L, Liu J, Gu X, Gong H, Shi X, Liu T, Wang C, Wang X, Liu G, Xing H. PEGylated WS2 nanosheets as a multifunctional theranostic agent for *in vivo* dual-modal CT/photoacoustic imaging guided photothermal therapy. Adv Mater 2014; 26:1886–93.
[17] Liu H, Neal AT, Zhu Z, Luo Z, Xu X, Tománek D, Ye PD. Phosphorene: an unexplored 2D Semiconductor with a high hole mobility. ACS Nano 2014;8:4033.
[18] Chen W, Ouyang J, Liu H, Chen M, Zeng K, Sheng J, Liu Z, Han Y, Wang L, Li J. Black phosphorus nanosheet-based drug delivery system for synergistic photodynamic/photothermal/chemotherapy of cancer. Adv Mater 2017;29: 1603864.
[19] Liu T, Wang C, Gu X, Gong H, Cheng L, Shi X, Feng L, Sun B, Liu Z. Drug delivery with PEGylated MoS2 nano-sheets for combined photothermal and chemotherapy of cancer. Adv Mater 2014;26:3433–40.
[20] Kuo WS, Lin YS, Wu PC, Chang CY, Wang JY, Chen PC, Hsieh MH, Kao HF, Lin SH, Chang CC. Two-photon–near infrared-II antimicrobial graphene-nanoagent for ultraviolet–near infrared imaging and photoinactivation. Int J Mol Sci 2022;23: 3230.
[21] Yadav V, Roy S, Singh P, Khan Z, Jaiswal A. 2D MoS2-based nanomaterials for therapeutic, bioimaging, and biosensing applications. Small 2019;15:1803706.
[22] Sweet C, Pramanik A, Jones S, Ray PC. Two-photon fluorescent molybdenum disulfide dots for targeted prostate cancer imaging in the biological II window. ACS Omega 2017;2:1826–35.
[23] Sun Z, Xie H, Tang S, Yu XF, Guo Z, Shao J, Zhang H, Huang H, Wang H, Chu PK. Ultrasmall black phosphorus quantum dots: synthesis and use as photothermal agents. Angew Chem Int Ed 2015;54:11526–30.
[24] Li X, Chen C, Yang Y, Lei Z, Xu H. 2D Re-based transition metal chalcogenides: progress, challenges, and opportunities. Adv Sci 2020;7:2002320.
[25] Kertesz M, Hoffmann R. Octahedral vs. trigonal-prismatic coordination and clustering in transition-metal dichalcogenides. J Am Chem Soc 1984;106:3453–60.
[26] Fang Y, Pan J, He J, Luo R, Wang D, Che X, Bu K, Zhao W, Liu P, Mu G. Structure re-determination and superconductivity observation of bulk 1T MoS2. Angew Chem 2018;130:1246–9.
[27] Tian H, Tice J, Fei R, Tran V, Yan X, Yang L, Wang H. Low-symmetry two-dimensional materials for electronic and photonic applications. Nano Today 2016; 11:763–77.
[28] Cui F, Li X, Feng Q, Yin J, Zhou L, Liu D, Liu K, He X, Liang X, Liu S, Lei Z, Liu Z, Peng H, Zhang J, Kong J, Xu H. Epitaxial growth of large-area and highly crystalline anisotropic $ReSe_2$ atomic layer. Nano Res 2017;10:2732–42.
[29] Jariwala B, Voiry D, Jindal A, Chalke BA, Bapat R, Thamizhavel A, Chhowalla M, Deshmukh M, Bhattacharya A. Synthesis and characterization of ReS2 and ReSe2 layered chalcogenide single crystals. Chem Mater 2016;28:3352–9.
[30] Rayman MP. Selenium in cancer prevention: a review of the evidence and mechanism of action. Proc Nutr Soc 2005;64:527–42.
[31] Jia X, Bai J, Ma Z, Jiang X. BSA-exfoliated WSe 2 nanosheets as a photoregulated carrier for synergistic photodynamic/photothermal therapy. J Mater Chem B 2017; 5:269–78.
[32] Li Y, Luo Z, Song Y, Yuan Y, Peng X, Song J, Qu J. Rhenium disulfide nanosheets as a promising probe for intracellular two-photon luminescence imaging. Sens Actuators B 2022;362:131781.
[33] Ran J, Chen L, Wang D, Talebian-Kiakalaieh A, Jiao Y, Adel Hamza M, et al. Atomic-level regulated 2D ReSe2: a universal platform boostin photocatalysis. Adv Mater 2023;35:2210164.
[34] Jiang S, Zhang Z, Zhang N, Huan Y, Gong Y, Sun M, Shi J, Xie C, Yang P, Fang Q, Li H, Tong L, Xie D, Gu L, Liu P, Zhang Y. Application of chemical vapor–deposited monolayer ReSe2 in the electrocatalytic hydrogen evolution reaction. Nano Res 2018;11:1787–97.
[35] Qi F, Wang X, Zheng B, Chen Y, Yu B, Zhou J, He J, Li P, Zhang W, Li Y. Self-assembled chrysanthemum-like microspheres constructed by few-layer ReSe2 nanosheets as a highly efficient and stable electrocatalyst for hydrogen evolution reaction. Electrochim Acta 2017;224:593–9.
[36] Wolverson D, Crampin S, Kazemi AS, Ilie A, Bending SJ. Raman spectra of monolayer, few-layer, and bulk $ReSe_2$: an anisotropic layered semiconductor. ACS Nano 2014;8:11154–64.
[37] Hafeez M, Gan L, Li H, Ma Y, Zhai T. Chemical vapor deposition synthesis of ultrathin hexagonal $ReSe_2$ flakes for anisotropic raman property and optoelectronic application. Adv Mater 2016;28:8296–301.
[38] Arao Y, Kubouchi M. High-rate production of few-layer graphene by high-power probe sonication. Carbon 2015;95:802–8.
[39] Tao Youtian, Yang C, Qin J. Organic host materials for phosphorescent organic light-emitting diodes. Chem Soc Rev 2011;40:2943–70.
[40] Shim M, Guyot-Sionnest P. N-type colloidal semiconductor nanocrystals. Nature 2000;407:981–3.
[41] Rong Y, Wu C, Yu J, Zhang X, Ye F, Zeigler M, Gallina ME, Wu IC, Zhang Y, Chan YH. Multicolor fluorescent semiconducting polymer dots with narrow emissions and high brightness. ACS Nano 2013;7:376–84.
[42] Kim E, Koh M, Lim BJ, Park SB. Emission wavelength prediction of a full-color-tunable fluorescent core skeleton, 9-aryl-1, 2-dihydropyrrolo [3, 4-b] indolizin-3-one. J Am Chem Soc 2011;133:6642–9.
[43] Gu W, Yan Y, Cao X, Zhang C, Ding C, Xian Y. A facile and one-step ethanol-thermal synthesis of MoS2 quantum dots for two-photon fluorescence imaging. J Mater Chem B 2016;4:27–31.
[44] Qian J, Dan W, Cai FH, Xi W, Li P, Zhu ZF, et al. Observation of multiphoton-induced fluorescence from graphene oxide nanoparticles and applications in *in vivo* functional bioimaging. Angew Chem 2012;124:10722–7.